Materials Advances

ROYAL SOCIETY OF CHEMISTRY

PAPER

View Article Online
View Journal | View Issue

Cite this: *Mater. Adv.*, 2023, 4, 1978

An electrically stable and mechanically robust stretchable fiber conductor prepared by dip-coating silver nanowires on porous elastomer yarn†

Xin He,[a] Ningjing Zhou,[a] Yushan Li,[a] Puxian Xiong,[a] Shuai Zhang*[c] and Zhijun Ma*[b]

Stretchable fiber conductors are promising for constructing high-performance wearable electronic devices due to their one-dimensional shape, small size, light weight, and excellent integrability. Here, we report the fabrication of a super stretchable fiber conductor by simply dip-coating silver nanowires (AgNWs) on electrospinning-derived porous poly(styrene-*block*-butadiene-*block*-styrene) (SBS) yarn. The stretchable fiber conductor is denoted as AgNWs@pSBS. This fiber possesses super stretchability and high electrical conductance. Compared with the fiber using nonporous elastomer fiber as the substrate, the AgNWs@pSBS fiber here possesses remarkably enhanced electrical stability and mechanical robustness. This fiber could be encapsulated by a porous elastomer sheath through *in situ* electrospinning of SBS microfibers for protection and insulation purpose, while its electrical stability and mechanical robustness could be further enhanced. With super stretchability, high conductivity, electrical stability, and mechanical robustness, the stretchable fiber conductor developed here is promising for transmission of electrical power or signals for wearable electronics. As a proof-of-concept, we demonstrate that, with a stretchable fiber conductor as the electrical circuit, an LED light and a loudspeaker could operate normally without obvious performance degradation irrespective of whether the fiber was relaxed or seriously deformed.

Received 7th January 2023,
Accepted 23rd March 2023

DOI: 10.1039/d3ma00013c

rsc.li/materials-advances

1. Introduction

Stretchable electronics are essential for practical wearable applications from personal healthcare, and human activity monitoring, to human–machine interfaces.[1–5] Traditional stretchable electronic devices were mostly made with a low-permeable elastomer (typically silicone rubber) film as the substrate, which is not ideal for wearable applications (requiring high breathability).[6–10] Recently, fiber-shaped stretchable electronic devices have been drawing more and more interest from academia and industry.[11–13] Compared with film-type devices, fiber-shaped devices are softer, lighter, and more compliant with the curvilinear surfaces of the human body.[14] Meanwhile, they can be conveniently integrated into various textiles without degrading the breathability and physical comfort of the substrates.[15,16] On the other hand, the fiber-shaped configuration is the ideal form for transmitting electrical power and signals, resembling the functionalities of traditional electrical wires. To date, various fiber-shaped stretchable devices, such as solar cells,[17–19] supercapacitors,[20,21] lithium–ion batteries,[22–24] sensors,[25–27] actuators,[28–30] *etc.*, have been reported.

As the basic building block of fiber-shaped stretchable electronic devices, stretchable fiber conductors have been drawing increasing research interest.[31] Their applications can be roughly divided into three categories: firstly, as a piezoresistive component for strain sensing;[32–34] secondly, as electrical wires for transmitting electrical power or signals;[35–39] thirdly, as an electrode of devices, such as solar cells, capacitors/supercapacitors, batteries, *etc.* for charge collection.[40–44] The first application requires stretchable fiber conductors with sensitive, wide-range, and linear piezoresistive properties to enable good strain-sensing performance. For the second and third applications, in addition to high stretchability and

[a] *State Key Laboratory of Luminescent Materials & Devices, Guangdong Engineering Technology Research and Development Center of Special Optical Fiber Materials and Devices, Guangdong Provincial Key Laboratory of Fiber Laser Materials and Applied Techniques, School of Materials Science and Engineering, South China University of Technology, Guangzhou 510641, China*
[b] *Research Center for Humanoid Sensing, Zhejiang Lab, Hangzhou, 311100, P. R. China. E-mail: zhijma@scut.edu.cn*
[c] *Zhejiang Chinese Medical University, Hangzhou, 311100, P. R. China. E-mail: zhsrenl@163.com*

† Electronic supplementary information (ESI) available. See DOI: https://doi.org/10.1039/d3ma00013c

conductivity, stretchable fiber conductors should have high electrical stability, *i.e.*, low resistance change during elongation, to enable stable working performance of the devices. Meanwhile, robust endurance to repeated deformation is also required to provide long-term stable operation. To date, some pioneering works regarding the preparation of stretchable fiber conductors with high electrical stability have been reported. For example, Z. Liu and R. H. Baughman *et al.* prepared super-stretchable conductive fiber with hierarchically buckled sheath by wrapping aligned carbon nanotube (CNT) sheets on pre-stretched elastomer fiber (pre-stretch and wrapping strategy).[45] By this strategy, a quality factor (Q value, the strain of the material divided by the resistance change of the material) of 421 at a strain of 905% was achieved. Similarly, a strain-insensitive fiber conductor with a worm-shaped buckled graphene microlayer sheath was prepared.[46] Although super-stretchability and very high electrical stability were achieved by the "pre-stretch and wrapping" strategy, it is difficult to obtain high conductivity due to the intrinsic low conductivity of CNTs and graphene sheets. Very recently, continuous fabrication of liquid metal sheath-core stretchable fiber that simultaneously possesses super-stretchability (1170% strain), high conductivity (4.35×10^4 S m^{-1}) and excellent electrical stability (4% resistance increase at 200% strain) was realized *via* a triaxial-nozzle wet spinning approach.[47] However, the insulating sheath of the fiber may bring about difficulty in electrical interconnection of the fibers or connecting with other electrical components.

Silver nanowires (AgNWs) have been employed as an excellent conductive reagent to fabricate stretchable fiber conductors due to their high conductivity and large aspect ratio. Meanwhile, controlled mass synthesis of AgNWs with excellent dispersing ability in water or alcohol could be achieved by a one-step polyol method.[48–50] The fabrication of stretchable fiber conductors with AgNWs was usually performed using a mixing strategy (dispersing AgNWs in an elastomer to form a mixture, which was then spun into fibers) or a coating strategy (coating AgNWs on the surface of elastomer fibers by dip-coating or spray-coating to form core-sheath fibers).[51–56] Compared with the mixing strategy, the coating strategy is easier to be implemented. In addition, as the AgNWs can contact with each other more closely without the spatial isolation from the elastomer matrix, it is much easier for this method to achieve high electrical conductivity. Nevertheless, the stretchability and electrical stability of such core-sheath fibers were usually poor due to irreversible microcracking of the AgNW sheath.

Here, we report the fabrication of a stretchable fiber conductor by dip-coating AgNWs on electrospinning-derived porous SBS yarn. The fiber was denoted as AgNWs@pSBS. Benefitting from the porous structure of the SBS yarn, in addition to super-stretchability (2970% strain) and low resistance (2.2 Ω cm^{-1}), the AgNWs@pSBS fiber also possesses high electrical stability (Q value = 0.22 at 114% strain) and mechanical robustness to repeated stretching, twisting, tearing, rubbing and long-time washing. Further enhancement of electrical stability and mechanical endurance could be achieved by coating an additional layer of SBS microfiber sheath on the fiber *via* post *in situ* electrospinning. As a proof-of-concept application, we demonstrate that the stretchable fiber here could provide reliable transmission of electrical power or signals to support stable operation of an LED light and a loudspeaker under serious deformation of the fiber.

2. Experimental methods

2.1 Fabrication of the AgNWs@pSBS fiber

SBS was dissolved in 1,2-dichloroethane (Macklin D807843-500 mL 107-06-2 AR, 99%) to form transparent and viscous solutions with concentrations of ~17 wt%, ~20 wt% and 25 wt % for electrospinning. A stainless-steel wire with a length of 50 cm and a diameter of 200 μm was used as a collector for collecting the electrospun SBS microfibers. By moving the nozzle back and forward during electrospinning, the microfibers could be deposited over the surface of the steel wire homogeneously. The collecting distance and applied voltage were set at 22.5 cm and 13.5 kV, respectively. The feeding rate of the SBS solution was set as 4 mL h^{-1}, 8 mL h^{-1} and 12 mL h^{-1}. After 5 minutes, the deposited SBS microfibers were peeled off from the metal wire to form a hollow-core porous yarn. The AgNW solution (XFNANO materials Tech Co., Ltd; average diameter and corresponding mean square error: ~76 nm and 0.19; concentration: 20 mg mL^{-1}; refer Fig. S1 (ESI†) for the micro-morphology and thickness distribution) was centrifuged for 5 minutes at 4000 rpm to remove the excess surfactant. Then isopropyl alcohol (Macklin1811925 CAS: 67-63-0 AR, ≥99.5%) with an equal volume to the removed supernatant was added to the AgNW solution. Finally, the electrospun SBS yarn was treated by dip-coating with the AgNW solution and thoroughly dried at room temperature for 10 minutes to obtain the AgNWs@pSBS fiber. The process for loading of AgNWs could be repeated to change the mechanical and electrical properties of the stretchable fiber conductors. The overall fabrication process of the AgNWs@pSBS fiber is schematically shown in Fig. 1(a). In fact, continuously long fiber can be fabricated by modifying the step for electrospinning preparation of the SBS yarn of the above strategy. As schematically illustrated in Fig. S2 (ESI†), after collection for certain time, when a desired diameter of the SBS yarn was achieved, about 80% length (40 cm) of the metal wire was extracted out of the SBS yarn (with ~10 cm left in the SBS yarn). Then the metal wire, with one end still being covered by ~10 cm length of SBS yarn, was used as the collector for collecting electrospun SBS fibers. The newly collected SBS yarn partly overlapped with the previously collected SBS yarn at one end of the metal wire (~10 cm) to form an integral yarn. The above operation was repeated to finally obtain a continuous SBS yarn with a desired length. Loading of AgNWs was performed with a similar operation process to the above mentioned. In this work, the concentration of the SBS solution and its feeding rate during electrospinning were varied, in order to investigate the influence of the porous nature of the electrospun SBS yarn on the mechanical and electrical properties of the AgNWs@pSBS fibers. Here, three kinds of SBS yarns were

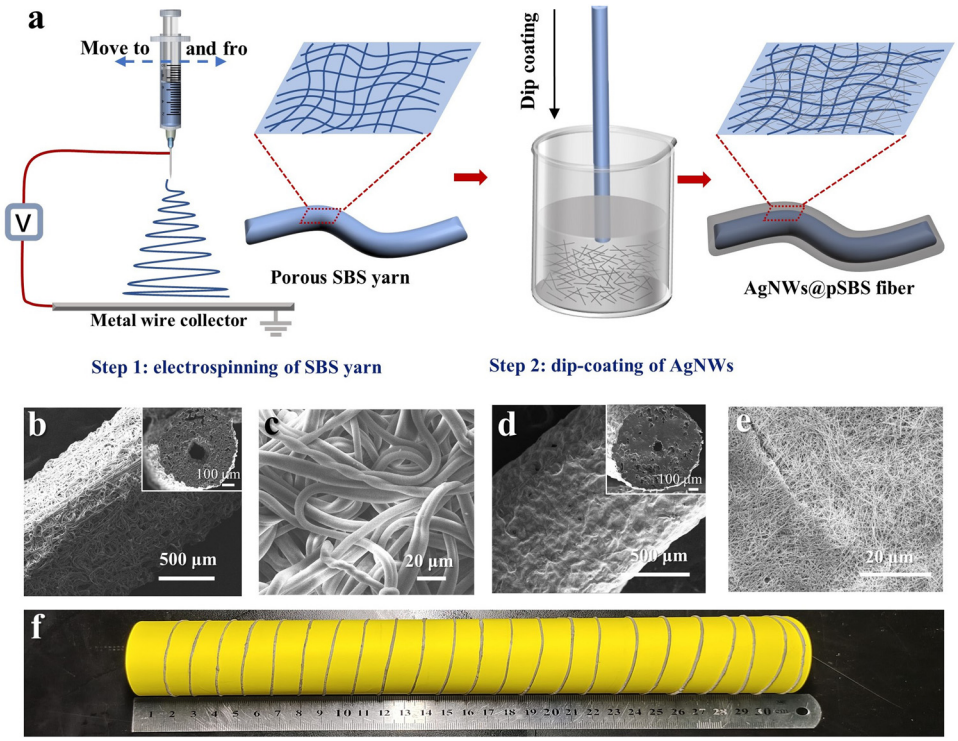

Fig. 1 (a) A scheme for fabrication of the AgNWs@pSBS fiber. (b)–(e) Scanning electron microscopy (SEM) images of a pSBS-20-8 yarn (b and c) and anAgNWs@pSBS-20-8 fiber (d and e) collected from the sidewall. (f) Photo of an AgNWs@pSBS-20-8 fiber with a length of ~3 m that is wound around a paper cylinder.

prepared and used as substrates for preparing AgNWs@pSBS fibers (3 cycles for dip-coating of AgNWs were employed). The concentrations of the SBS solution for these three yarns were ~17 wt%, ~20 wt% and 25 wt%, while the feeding rates of SBS solution during electrospinning were 4 mL min^{-1}, 8 mL min^{-1} and 12 mL min^{-1}, respectively. The corresponding SBS yarns were termed as pSBS-17-4, pSBS-20-8 and pSBS-25-12, while the corresponding AgNWs-pSBS fibers were termed as AgNWs@pSBS-17-4, AgNWs@pSBS-20-8 (typical sample throughout the manuscript) and AgNWs@pSBS-25-12 (the numbers 17, 20 and 25 refer to the concentrations of SBS solution, while the numbers 4, 8, and 12 refer to the feeding rate of SBS solution in electrospinning).

2.2 Encapsulation of the AgNWs@pSBS fiber

Encapsulation of the AgNWs@pSBS fiber was performed by *in situ* deposition of electrospun SBS microfibers using an AgNWs@pSBS-20-8 fiber as the collector. Briefly, two pieces of copper wires (0.08 mm in diameter) were wound on both ends of an AgNWs@pSBS-20-8 fiber. The fiber was hanging parallel to the ground by fastening the copper wires on its ends to one pair of iron supports. The collecting distance, applied voltage and feeding rate of the SBS solution were set as 22.5 cm, 13.5 kV and 8 mL h^{-1}, respectively. After tuning the direction of the spinning nozzle to a suitable angle (perpendicular to the AgNWs@pSBS-20-8 fiber), the electrospinning of SBS microfibers was performed. After electrospinning for 5 minutes, an encapsulated AgNWs@pSBS-20-8 fiber was prepared, which was termed as pSBS@AgNWs@pSBS.

2.3 Fabrication of the nonporous stretchable fiber conductor (as a control)

First, a nonporous SBS fiber was prepared by a multi-material thermal drawing method.[57] Briefly, an SBS rod with a diameter of 19.5 mm was inserted into a PMMA tube with a diameter of 30 mm and a wall thickness of 5 mm to form a PMMA@SBS preform with a core@clad structure. Then the SBS@PMMA preform was thermally drawn into a continuous fiber with a diameter of ~930 μm on a home-made fiber drawing tower. The composite SBS@PMMA fiber was treated by soaking in acetic acid at a temperature of 60 °C for 30 min to remove the PMMA clad. The obtained SBS fiber was rinsed with ethanol and thoroughly dried in an oven. Finally, the nonporous SBS fiber with similar experimental parameters to those of the AgNWs@pSBS fiber was treated by dip-coating for loading AgNWs. The nonporous fiber was termed as AgNWs@npSBS.

2.4 Characterization

Scanning electron microscopy (SEM, Quanta200, Hitachi) was used to investigate the micromorphology of the samples. To obtain a fresh cross-section, we first soaked the samples in liquid nitrogen and then cut the samples with a surgical blade after the samples became crisp. All the SEM images were collected in secondary electron mode with a working voltage of 10–20 V. In addition, we also obtained the elemental distribution at the cross section of the samples by electron diffuse spectroscopy (EDS) working in a 2D scanning mode. The porosity of the pSBS

yarns, AgNWs@pSBS fibers and pSBS@AgNWs@pSBS fibers was measured by a mercury intrusion method with high-performance automatic mercury intrusion equipment AutoPore V9620. Five 8.8 cm-length AgNWs@pSBS-20-8 or pSBS@AgNWs@pSBS fibers were prepared for measurement. The volume of the pore can be obtained by measuring the amount of mercury entering the pore under different external pressures. The larger the pressure is, the smaller the pore size is. The porosity is calculated by the following formula:

$$Pr = 2\gamma \cos\theta$$

where P is the external pressure applied by the equipment, r is the pore size of the porous structure into which the external pressure enters, θ is the contact angle of mercury to the solid, and γ is the surface tension of the mercury.

The mechanical properties of the samples were tested with an Instron 5599 universal testing system. To investigate the maximal stretchability of the fibers, all the samples were continuously stretched with a speed of 60 mm min^{-1} to the breaking strain to obtain the stress–strain curves. The stress–strain hysteresis curves of an AgNWs@pSBS-20-8 fiber with a free length of ~3 cm were also recorded under different strains (the stretching speed was also 60 mm min^{-1}).

The electromechanical properties of AgNWs@pSBS, pSBS@AgNWs@pSBS and AgNWs@npSBS fibers were measured with a homemade system composed of a computer-controlled stretching machine and a Keithley 2400 source meter. First, the fibers were cut into short pieces of approximately 2 cm in length. After fixing the samples on the stretching machine, silver paste was applied on both ends of the fibers to ensure good electrical contact during the measurement. During stretching, the resistance variation of the samples was simultaneously monitored and recorded using a computer. The resistance–strain hysteresis nature of an AgNWs@pSBS-20-8 fiber under different strains was also studied in a similar way. To investigate the robustness to torsion, the samples with a length of ~5 cm were repeatedly twisted with a degree of 360° using a motor-controlled rotator. During twisting, the resistance changes of the fibers were monitored using a Keithley 2400 source meter and recorded using a computer.

Specifically, the anti-rubbing test was carried out according to the International Organization for Standardization (ISO 105). First, the fibers with copper wire electrodes on both ends were fixed, by an adhesive tape, to a steel ruler with a weight of 65 g. During the test, the steel ruler was moved on a Chinlon cloth with the fiber side contacting the cloth. Each cycle, the ruler was moved by 10 cm, after which, the resistance of the fibers was measured.

The anti-tearing test of fibers was performed according to ASTM D903 standard. First, the fibers were fixed with a double-sided adhesive tape on a steel plate, and then a piece of 3M scotch tape was neatly attached onto the top side of the fibers. A counterweight (500 g) was put on the scotch-tape-covered fiber for 30 s to ensure tight combination of the scotch tape and the fibers. The scotch tape was then peeled off from the fibers with a constant separation rate of 2.5 mm s^{-1}. After each cycle, the resistance of the samples was measured.

For the anti-washing test, the fibers with both ends wound by one pair of copper wires as the electrodes were soaked in water in a glass beaker and agitated with a magnetic stirrer at a speed of ~750 rpm at room temperature. The resistance of the samples was measured after every 10 minutes of washing, and the whole process took 2 h.

For wearable electronic devices in daily use, the influence from human body perspiration and liquids from the environment should be taken into consideration seriously. Here, endurance to sweat and water of the pSBS@AgNWs@pSBS fiber was investigated. First, the water contact angle on the pSBS@AgNWs@pSBS fiber was measured using an OCA40 Micro surface tension and contact angle tester. Then, 2 pieces of pSBS@AgNWs@pSBS fibers with end winded by a copper wire as the electrode were plied together, and then soaked in artificial sweat with a pH value of 5.5 or tap water. The electrical resistance between the fibers was monitored using a Keithley 2400 source meter and recorded using a computer. After soaking for 10 h, the plied fibers were picked out and completely dried for another test.

3. Results and discussion

The pSBS-20-8 yarn with a hollow core (formed due to extraction of the metal wire collector) was composed of electrospun SBS microfibers with an average thickness of ~7.3 μm (Fig. 1(b) and (c)). As the ultra-long AgNWs adhered compliantly to the rugged surface of the SBS yarn, the AgNWs@pSBS-20-8 fiber presented a wrinkled appearance. Meanwhile, the random stacking of the AgNWs imparts the fiber with another level of porosity with an average pore size of ~350 nm, which is also important to improve the permeability of the fiber (Fig. 1(d) and (e)). By a mercury intrusion method, the porosity of the AgNWs@pSBS-20-8 fiber was measured as ~69% with a pore size distribution mainly in the range of 2–100 μm (Fig. S3, ESI†). Such a porous structure, on one hand, endowed the fiber with high permeability to allow good wearing comfort. On the other hand, it could impart the AgNWs@pSBS-20-8 fiber with a very low volume density of 0.37 g cm^{-3}, being much lower than stainless-steel wire (3.16 g cm^{-3}), commercial cotton yarn (0.68 g cm^{-3}), chinlon yarn (1.32 g cm^{-3}), and polyester yarn (1.27 g cm^{-3}) (Fig. S4, ESI†). The AgNWs@pSBS-20-8 fiber possesses a round-shape cross-sectional configuration, and its average diameter and the corresponding mean square error (MSE) were measured as ~1.3 mm and 0.05 (Fig. S5 and Table S1, ESI†). By using a lab-scale electrospinning machine, we have been able to fabricate a continuous AgNWs@pSBS-20-8 fiber with a length of ~3 meters (3 cycles treated) (Fig. 1(f)).

The properties of the AgNWs-pSBS fibers could be tuned by the porosity of the SBS yarn and the dip-coating cycles for loading AgNWs. We first investigate the influence from the porosity of the SBS yarn, which was varied by changing the concentration of SBS solution and its feeding rate in electrospinning. Both high concentration and high feeding rate of the

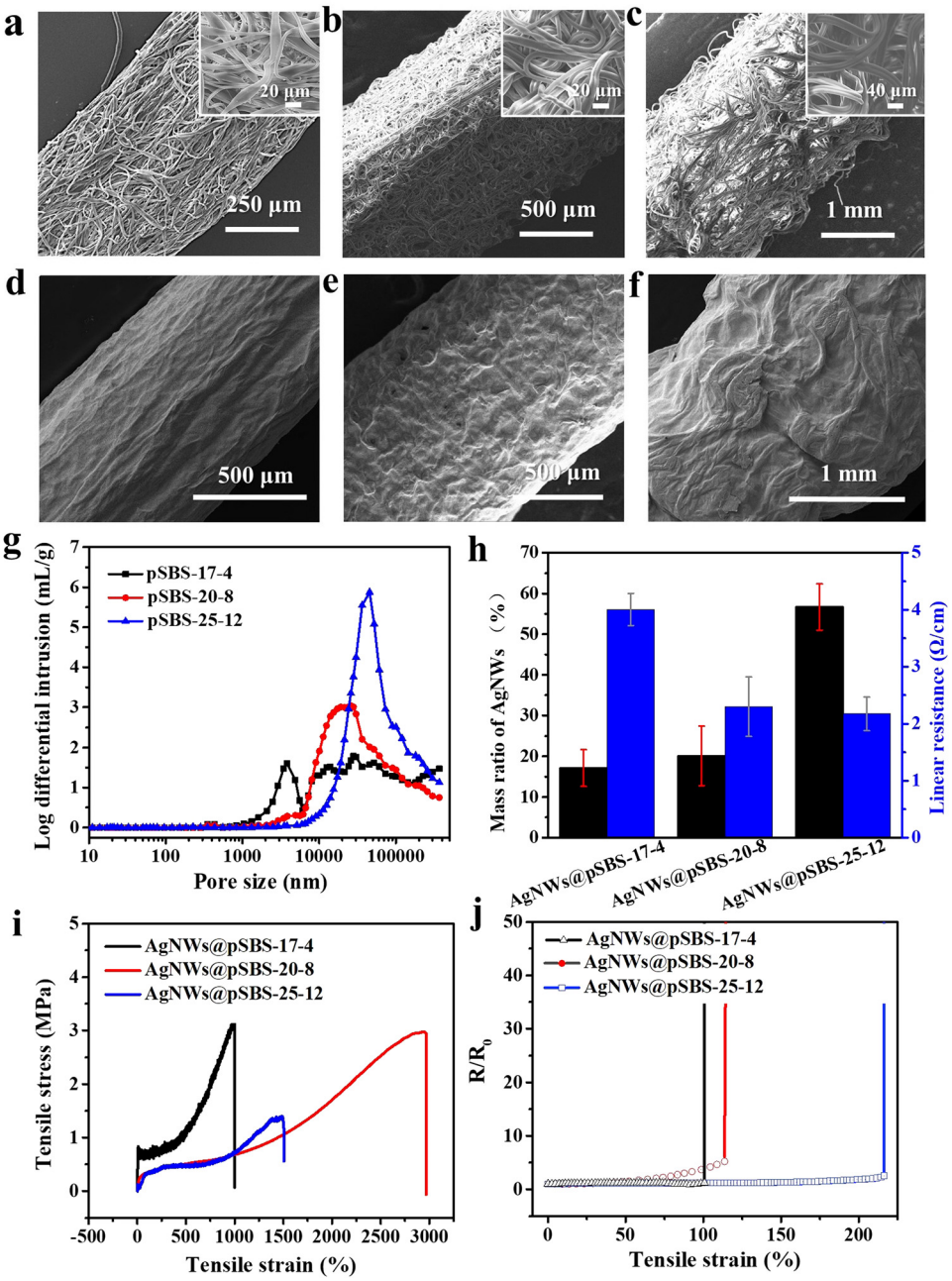

Fig. 2 (a)–(c) SEM images of pSBS-17-4, pSBS and pSBS-25-12 yarns. (d)–(f) SEM images of AgNWs@pSBS-17-4, AgNWs@pSBS-20-8 and AgNWs@pSBS-25-12 fibers. (g) Pore size distribution curves of pSBS-17-4, pSBS-20-8 and pSBS-25-12 yarns. (h) Mass ratio of AgNWs and linear resistance of AgNWs@pSBS-17-4, AgNWs@pSBS-20-8 and AgNWs@pSBS-25-12 fibers. (i) and (j) stress–strain curves and resistance curves of AgNWs@pSBS-17-4, AgNWs@pSBS-20-8 and AgNWs@pSBS-25-12 fibers.

SBS solution are beneficial to increase the thickness of electrospun SBS fibers and diameter of the final SBS yarns, which in turn influence the porosity of the SBS yarns. The diameters of pSBS-17-4, pSBS-20-8 and pSBS-25-12 yarns were measured as 0.7 mm, 1.2 mm and 1.8 mm, while the corresponding thickness of the electrospun SBS fibers was 3.7 μm, 7.3 μm and 11.9 μm, respectively. The pore size and porosity of the yarns also increased with the increase of concentration and feeding rate of SBS solution (Fig. 2(g)), which was beneficial to increase the mass loading of AgNWs, thus enhancing the conductivity of the fibers. Mass loadings of AgNWs on AgNWs@pSBS-17-4, AgNWs@pSBS-20-8 and AgNWs@pSBS-25-12 were 17.1 wt%, 20.2 wt% and 56.9 wt%, while linear resistance of the fibers was 4.1 Ω cm^{-1}, 2.4 Ω cm^{-1} and 2.1 Ω cm^{-1}, respectively (Fig. 2(h)). Larger pore size and higher porosity also contributed to improving the electrical stretchability and stability of the fibers (the critical strain, above which resistance increases abruptly, for AgNWs@pSBS-17-4, AgNWs@pSBS-20-8 and AgNWs@pSBS-25-12

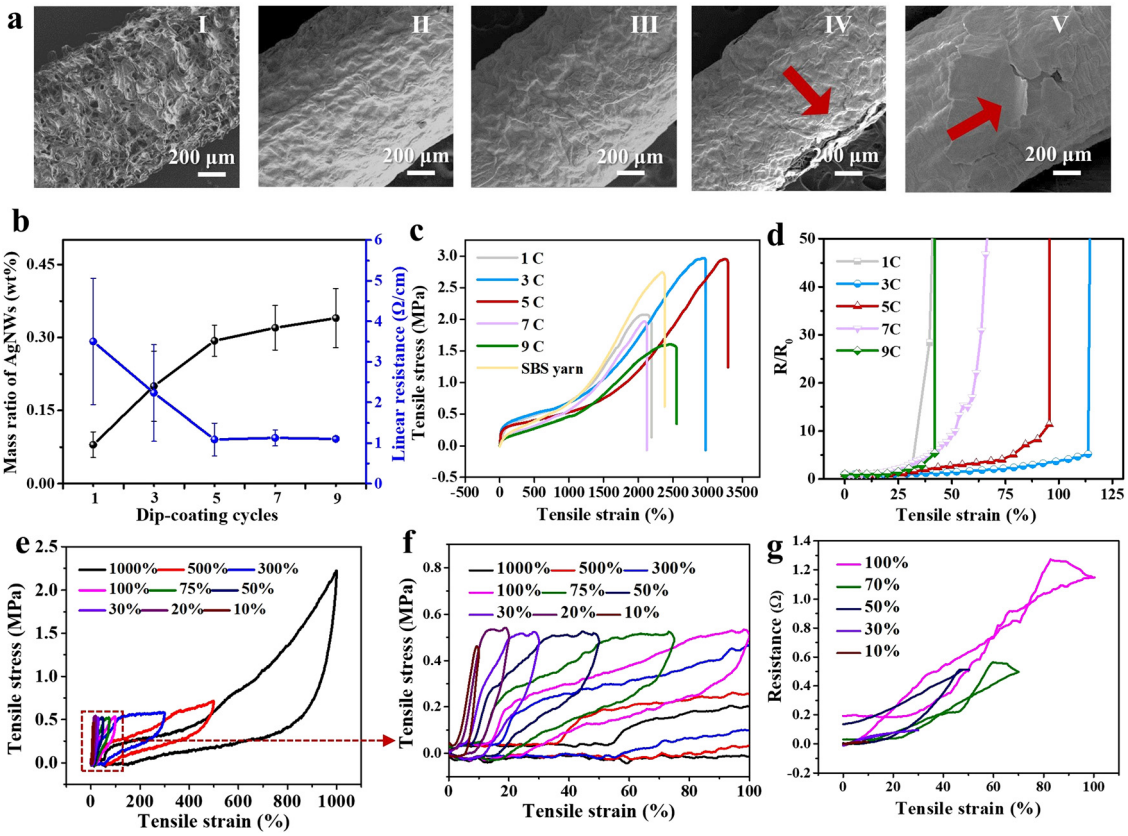

Fig. 3 Surface SEM images (a), variation of mass ratio of AgNWs and conductivity (b), stress–strain curves (c), and resistance change during stretching (d) of the AgNWs@SBS fibers with different treating cycles for loading AgNWs. (e) and (f) Stress–strain hysteresis curves of the AgNWs@SBS-20-8 fiber under different strains. (g) Resistance–strain hysteresis cures of the AgNWs@SBS-20-8 fiber under different strains.

fibers was 100%, 114% and 216%), despite the highest mechanical stretchability being achieved by the AgNWs@pSBS-20-8 fiber (the strain at break of AgNWs@pSBS-17-4, AgNWs@pSBS-20-8 and AgNWs@pSBS-25-12 fibers was 1001%, 2970% and 1510%) (Fig. 2(i) and (j)).

Loading of AgNWs, on one hand, could enhance the electrical conductivity. On the other hand, it could also influence the mechanical stretchability of the AgNWs@pSBS fiber. Mass loading of AgNWs on the AgNWs@pSBS fiber could be changed by varying the repeating cycles of the dip-coating process (Fig. 3(a) and the black curve in Fig. 3(b)), which is the key strategy for tuning the electrical and electromechanical properties of the fiber, now that a commercial AgNW suspension with a determined concentration of 20 mg mL^{-1} was used throughout this work. 1 cycle of dip-coating only led to partial coverage of AgNWs on the AgNWs@pSBS fiber (Fig. 3(a)-I). When the dip-coating was increased to 3 cycles, full coverage of AgNWs could be achieved (Fig. 3(a)-II). More cycles of dip-coating could further increase the mass loading of AgNWs. However, the overloading of AgNWs led to their local detachment from the fiber's surface (pointed by the red arrows in Fig. 3(a)-IV, V). The electrical resistance of the AgNWs@pSBS fiber decreased linearly with the increase of dip-coating cycles, which saturated at 5 cycles with a resistance value of 1.1 Ω cm^{-1}. Further increase of dip-coating cycles failed to further decrease the resistance, which is possibly ascribed to the local detachment of AgNWs (the blue curve in Fig. 3(b)). The mechanical stretchability of the fiber also increased with the repeating of the dip-coating process before 5 cycles. The maximal strain of the 1-cycle, 3-cycles, and 5-cycles treated samples was ~2190%, ~2970%, and ~3290%. The enhanced stretchability of the AgNWs@pSBS fiber, we assume, should be ascribed to the strengthening effect from the random network of the AgNWs. However, due to the local detachment of AgNWs, further increasing the dip-coating process to 7 cycles and 9 cycles, in contrast, led to a decrease of the maximal strain to ~2120% and ~2550%, respectively (Fig. 3(c)). Variation rule of the electromechanical properties of the AgNWs@pSBS presented a similar trend to that of the mechanical stretchability, but the critical strain (the strain above which burst increase of electrical resistance happens) and highest electrical stability were achieved by the 3-cycle treated sample (Fig. 3(d)). Therefore, 3 cycles of dip-coating should be adopted as an optimized parameter for preparing the AgNWs@pSBS fiber when both high conductivity and electrical stability are desired. As shown in Fig. 3(e) and (f), the stress–strain curves of the 3-cycle treated AgNWs@pSBS-20-8 fiber during repeated stretching–releasing cycles under different strains demonstrated obvious hysteresis character, which may be ascribed to the delayed shape recovery of the SBS yarn. In addition, relaxing behavior of the fiber occurred

when the strain was higher than 50%. Electrical hysteresis of the fiber began to appear at higher strains than the stress. The resistance–strain curves at the stretching and releasing stages overlapped neatly when the strains were lower than 30%, but obvious hysteresis loops appeared at strains of 50%, 70% and 100% (Fig. 3(g)). Therefore, when designing soft electronic devices and systems, the mechanical and electrical hysteresis properties of the AgNWs@pSBS fibers should be taken into consideration seriously.

It is interesting to notice that the porous structure of the SBS yarn plays an important role in enhancing the electrical properties and mechanical endurance of the AgNWs@pSBS fiber. When we used a nonporous SBS fiber to replace the porous SBS yarn (with a similar diameter to the SBS yarn, the corresponding sample was termed as AgNWs@npSBS), with the same 3 cycles of dip-coating, the mass loading of AgNWs on the fiber was ~5.6 wt%, only ~28% percent of the AgNWs@pSBS-20-8 fiber (20.2 wt%), while its linear resistance (29.5 Ω cm^{-1}) was ~13 times of that of the AgNWs@pSBS-20-8 fiber (2.2 Ω cm^{-1}). In addition to high conductivity, electrical stability and mechanical endurance of the AgNWs@pSBS-20-8 fiber were also enhanced substantially compared with the nonporous fiber. After being stretched to 114% of the original length, its resistance only increased by 4.2 times, corresponding to a *Q*

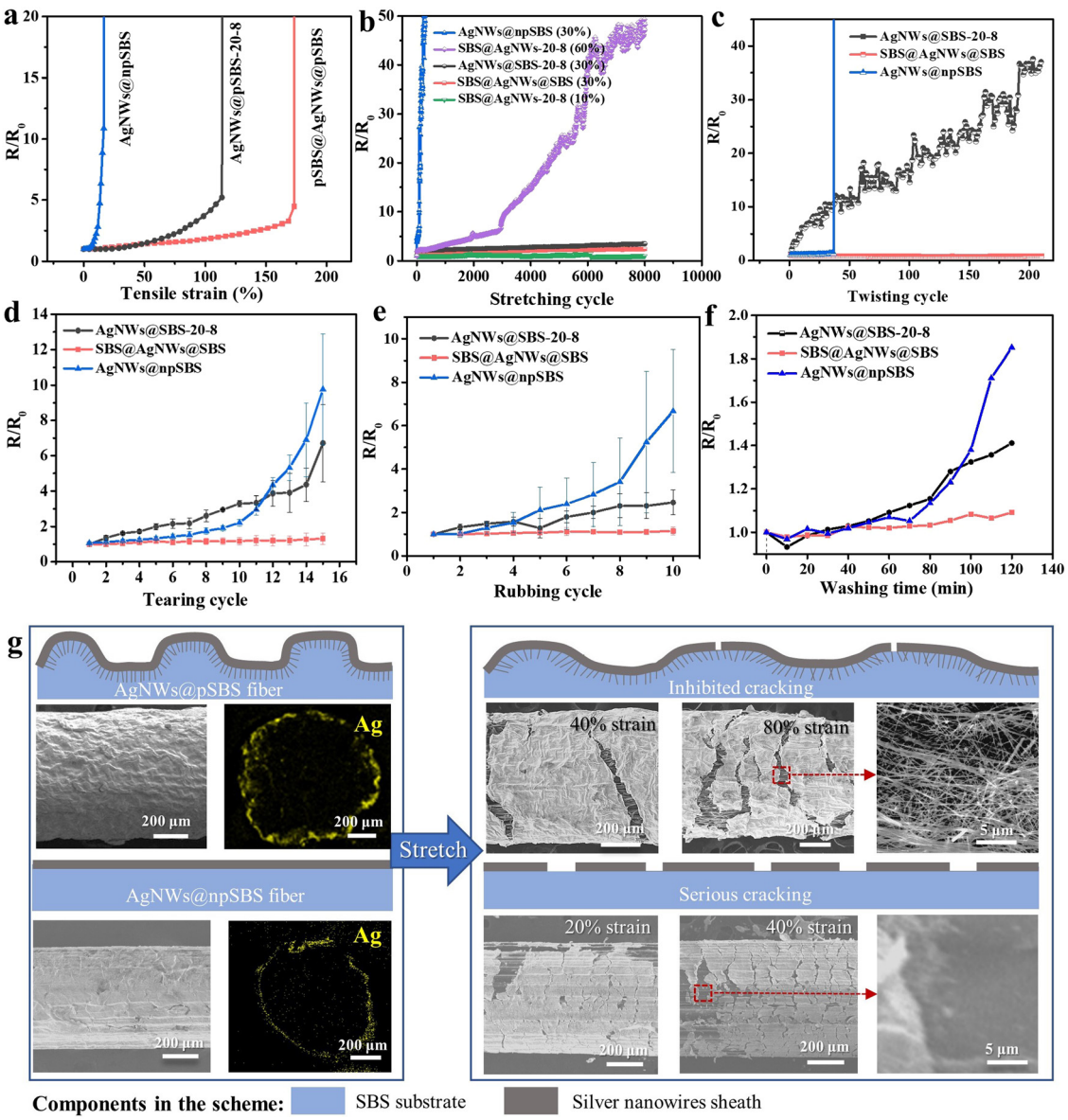

Fig. 4 (a) Resistance change of the AgNWs@npSBS (blue curve), AgNWs@pSBS-20-8 (black curve) and pSBS@AgNWs@pSBS (red curve) fibers as a function of applied strain. (b)–(f) Resistance change of the AgNWs@npSBS (blue curve), AgNWs@pSBS-20-8 (black curves) and pSBS@AgNWs@pSBS (red curves) fibers during repeated stretching (b), twisting (c), tearing (d), rubbing (e) and long-time washing (f). (g) A scheme and experimental evidence illustrating the mechanism for the enhancement of the electrical stability and mechanical endurance of the AgNWs@pSBS fiber. The scheme shows the cross-sectional structures of the fibers along the length direction.

value of 0.22 (Fig. 4(a)). This level of electrical stability has surpassed most of the yet reported stretchable fiber conductors with AgNWs as the conductive reagent (Table 1).[51–53,55,56,58–60] The AgNWs@pSBS-20-8 fiber could bear 8000 cycles of stretching with only 1% resistance increase at a strain of 10% or with a 2.5 fold resistance increase at a strain of 30%, while the nonporous fiber could only bear 500 cycles of stretching at a strain of 30% with ~18 500 fold resistance increase. When the stretching strain was increased to 60%, the AgNWs@pSBS-20-8 fiber could still bear 8000 cycles of stretching with less than 50 fold resistance increase (Fig. 4(b)); under the same twisting test (360°), the AgNWs@pSBS-20-8 fiber could bear 200 cycles with 34 fold resistance increase; however, the nonporous fiber became insulating after only 37 cycles of twisting (the black and blue curves in Fig. 4(c)). In addition to stretching and twisting, the porous fiber also performed better in repeated tearing (with 3M scotch tape), rubbing (on Chinlon cloth) and long-time washing (120 min) (black and blue curves in Fig. 4(d)–(f)). As illustrated in Fig. 4(g), the improved electrical stability and mechanical endurance of the AgNWs@pSBS fiber should be ascribed to two factors. First, the AgNW sheath of the AgNWs@pSBS fiber presented a wrinkled structure caused by the rugged surface of the porous SBS yarn. Such a wrinkled structure can effectively release tensile strain during stretching. Secondly, also more importantly, part of the under-layer AgNWs penetrated deep into the porous structure of the SBS yarn (which cannot be achieved by the nonporous fiber), behaving like plant roots that firmly grab the substrate thus inhibiting the generation and extension of microcracks (the EDS mapping results in Fig. 4(g)). A similar phenomenon has been reported

Table 1 Comparison of the electrical stability of the AgNWs@pSBS fiber and those from previously reported works

Fiber form	R/R_0	Strain (%)	Q value	Ref.
SBS fiber dispersed with AgNWs and coated with AgNP sheath	$>10^4$	112	$<10^{-4}$	51
TPU fiber dispersed with AgNWs and CNTs	>12	125	~0.1	52
TPU fiber dispersed with AgNWs	10^6	170	10^{-6}	53
PU cord coated with buckled AgNW sheath	6	134	~0.22	55
(AgNW)/polyurethane composite fiber with a buckled sheath-core architecture	1.5	150	1	56
PU hollow fiber with AgNWs coated on the inside wall	>50	100	0.02	58
Epoxy/NBR electrospun fibers spray-coated with AgNW/PU composites	4.7	80	0.17	59
Commercial elastomer yarn coated with AgNWs	2.0	30	0.15	60
Elastomer yarn coated with AgNWs	5.2	114	0.22	This work

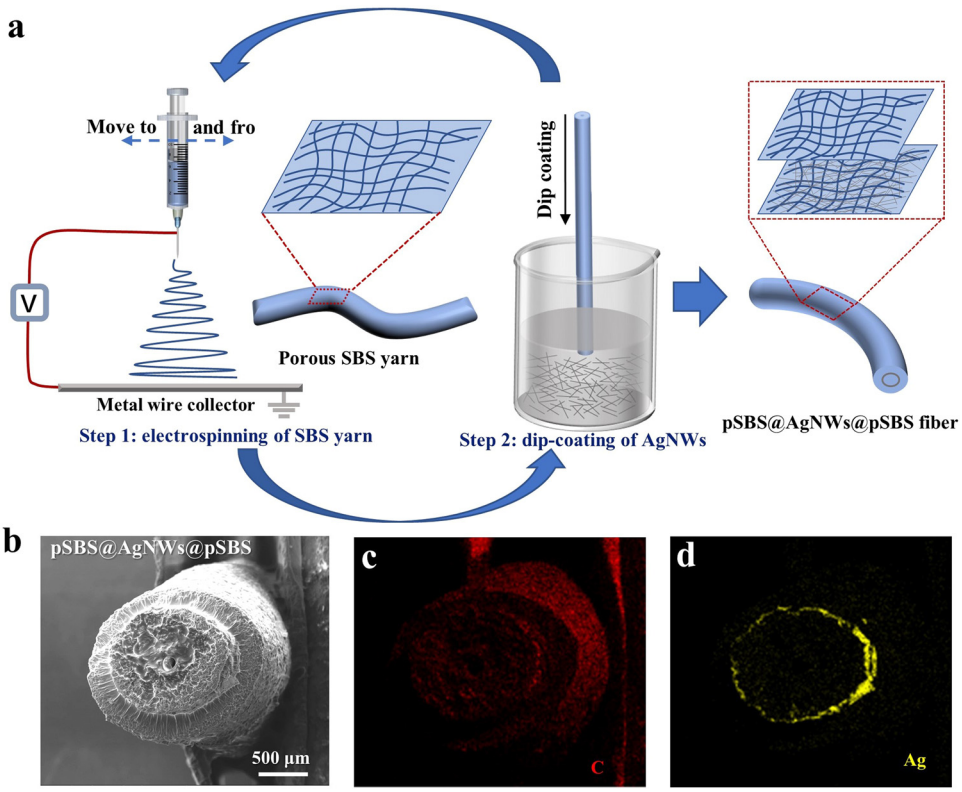

Fig. 5 (a) A scheme for the fabrication of the pSBS@AgNWs@pSBS fiber. (b)–(d) Cross-sectional SEM images and EDS patterns of the pSBS@AgNWs@pSBS fiber.

Table 2 Resistance increase of different fibers after various mechanical tests

Samples	RI (stretch)	RI (twist)	RI (tear)	RI (rub)	RI (wash)
AgNWs@npSBS	1.9×10^4 (500 cycles)	1.2×10^7 (37 cycles)	9.7 (15 cycles)	6.7 (10 cycles)	1.9 (120 min)
AgNWs@pSBS-20-8	3.5 (8000 cycles)	37.0 (210 cycles)	2.2 (15 cycles)	2.5 (10 cycles)	1.4 (120 min)
pSBS@AgNWs@pSBS	2.5 (9700 cycles)	0.8 (210 cycles)	1.3 (15 cycles)	1.1 (10 cycles)	1.1 (120 min)

RI: resistance increase of the fibers after different mechanical tests, calculated by: R/R_0 (R refers to the resistance after the test, R_0 refers to the resistance before the test).

by Y. Zhao and W. Cheng *et al.*, wherein gold nanowires played the role of "plant roots" and the electroless coated gold film acted as the role of "on-ground body of plant".[61] Also evidenced by the SEM images in Fig. 4(g), compared with the AgNWs@npSBS fiber, the cracking of the AgNW sheath on the AgNWs@pSBS-20-8 fiber was significantly inhibited. According to a statistical result, the number of cracks on the porous fiber at 80% strain was only 23 cm, while the number on the nonporous fiber at 40% strain has surpassed 90 cm. After releasing of the strain, debris of the cracked AgNWs sheath on the AgNWs@pSBS-20-8 fiber could contact each other again to restore the electrical conductivity (Fig. S6, ESI†). Therefore, employing a porous elastomer yarn as the substrate, here, is the key factor to obtain a stretchable fiber conductor with enhanced electrical and mechanical properties.

The additive deposition process of electrospinning makes it convenient to perform post-encapsulation of the AgNWs@pSBS fiber with a porous elastic sheath for protection and insulation purpose. By using an AgNWs@pSBS-20-8 fiber as the collector during electrospinning, electrospun SBS microfibers could be deposited on the surface of the fiber by strong electrostatic attraction to form a porous sheath (Fig. 5). The encapsulated fiber was denoted as pSBS@AgNWs@pSBS, and its electromechanical properties and robustness were investigated in various mechanical tests. Compared with the non-encapsulated AgNWs@pSBS-20-8 fiber, the critical strain of the encapsulated fiber was improved by 60% (from ~114% to ~173%), while its Q value at the critical strain increased by 130% (from ~0.22 to ~0.51) (the red curve in Fig. 4(a)). In addition to electrical stability, mechanical endurance of the encapsulated fiber, including in repeated stretching, twisting, tearing, rubbing and long-time washing, was also remarkably enhanced. Specifically, except the repeated stretching test, the resistance increase of the encapsulated fiber after different tests (twisting, tearing, rubbing and washing) could be inhibited below 8% (the red curves in Fig. 4(b)–(f)). Table 2 summarizes the performance of the fibers in different mechanical tests. Moreover, after encapsulation of the SBS microfibrous sheath, the entirely porous properties of the fiber could be well retained (Fig. S7, ESI†). Indeed, the porous structure of the fiber may cause additional concern brought by the invasion of human perspiration and environmental liquids. Fortunately, the electrospun SBS yarn here demonstrated high hydrophobicity (water contact angle: ~130°, Fig. S8a, ESI†), which can block the penetration of sweat and

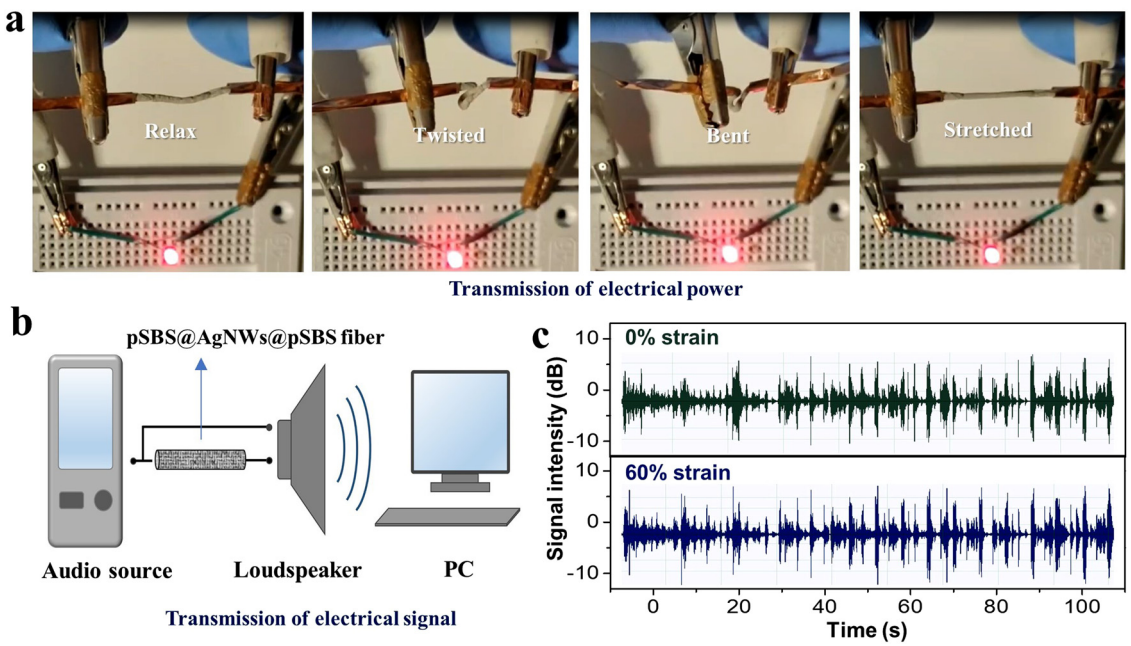

Fig. 6 (a) Luminescence of an LED with an AgNWs@pSBS-20-8 fiber as part of the electrical circuit. (b) A scheme showing the wiring of the setup for demonstrating the application of the fiber in audio signal transmission. (c) The waveform of the transmitted audio signal with a pSBS@AgNWs@pSBS fiber at relaxation and under 60% strain, respectively.

water. Excellent electrical insulation between one pair of plied pSBS@AgNWs@pSBS fibers was well retained after soaking in artificial sweat or tap water for 10 h (Fig. S8b–d, ESI†).

Stretchable fiber conductors with both high electrical conductivity and stability is advantageous for transmission of electrical power or signals in stretchable electronic devices, wherein low intensity attenuation and high transmission fidelity are required. As a proof of concept, here we demonstrate two simple application examples. First, a piece of AgNWs@pSBS-20-8 fiber was used in an electrical circuit for transmitting electrical power to light an LED chip. Irrespective of whether the AgNWs@pSBS-20-8 fiber was relaxed, stretched, bent or twisted seriously, the LED chip could glow normally without obvious fading of luminescence intensity (Fig. 6(a)). In the second example, we employed a pSBS@AgNWs@pSBS fiber as a stretchable cable for transmission of audio signals. As shown in Fig. 6(b) and (c), both configuration and intensity of the audio signal's waveform transmitted by the fiber at relaxation or under 60% strain were very similar. Therefore, the stretchable fiber conductors developed here are reliable as an electrical power or signal transmission wire for wearable electronics.

4. Conclusions

In summary, we propose a strategy for fabricating stretchable fiber conductors by dip-coating AgNWs on electrospinning-derived SBS yarn. Due to the porous structure of the SBS yarn, the AgNW sheath on the fiber formed a wrinkled structure with part of the under-layer AgNWs penetrating into the substrate, which imparts the fiber with high electrical stability (Q value: 0.22). The porous structure also substantially reduces the volume density of the fiber to lower than those of various commercial yarns, which is beneficial to improve its wearing comfort in wearable applications. In addition to high electrical stability and low volume density, the stretchable fiber conductor also possesses super elasticity (strain-at-break: 2970%), low resistance (2.2 Ω cm^{-1}), and high electrical stretchability (critical strain: 114%). Meanwhile, it is resilient to various mechanical reliability tests, including repeated stretching, twisting, tearing and rubbing, as well as long-time washing.

The electrical stability and mechanical robustness of the stretchable fiber conductor could be remarkably enhanced by encapsulation of SBS microfibers on the surface. The Q value at critical strain of the encapsulated fiber increased by 130% compared with that of the non-encapsulated fiber. Its resistance increase was inhibited by lower than 8% after repeated twisting, tearing, rubbing, or long-time washing. In addition, the porous SBS sheath, with high hydrophobicity, could also provide insulation and protection effects to the fiber. Benefitting from the high electrical conductivity and stability, the stretchable fiber conductor developed here is advantageous in constructing stretchable electrical circuits. As a proof of concept, we demonstrated that both an LED and a loud speaker could operate stably when using a stretchable fiber conductor for transmitting electrical power or signals, irrespective of whether the fiber was relaxed or deformed seriously.

Author contributions

Conceptualization: Zhijun Ma and Xin He; experiments: Xin He, Ningjing Zhou, and Yushan Li; writing – original draft: Zhijun Ma, Xin He, and Puxian Xiong; visualization: Zhijun Ma, Xin He, and Shuai Zhang; supervision: Zhijun Ma.

Conflicts of interest

There are no conflicts of interest to declare.

Acknowledgements

This work was financially supported by the Key R&D Program of Guangzhou (no. 202007020003), the Research project of Zhejiang Lab (no. 113014-AC2101), and the National Natural Science Foundation of China (grant no. 51872095).

References

1 S. Yao, P. Swetha and Y. Zhu, *Adv. Healthcare Mater.*, 2018, **7**, 1700889.
2 S. Yao, P. Ren, R. Song, Y. Liu, Q. Huang, J. Dong, B. T. O'Connor and Y. Zhu, *Adv. Mater.*, 2020, **32**, 1902343.
3 M. A. A. Mamun and M. R. Yuce, *Adv. Funct. Mater.*, 2020, **30**, 2005703.
4 H. Wang, X. Ma and Y. Hao, *Adv. Mater. Interfaces*, 2017, **4**, 1600709.
5 S. Gong, L. W. Yap, B. Zhu and W. Cheng, *Adv. Mater.*, 2020, **32**, 1902278.
6 Z. Huang, Y. Hao, Y. Li, H. Hu, C. Wang, A. Nomoto, T. Pan, Y. Gu, Y. Chen, T. Zhang, W. Li, Y. Lei, N. Kim, C. Wang, L. Zhang, J. W. Ward, A. Maralani, X. Li, M. F. Durstock, A. Pisano, Y. Lin and S. Xu, *Nat. Electron.*, 2018, **1**, 473–480.
7 S. Liu, D. S. Shah and R. Kramer-Bottiglio, *Nat. Mater.*, 2021, **20**, 851–858.
8 G. Shi, Z. Zhao, J.-H. Pai, I. Lee, L. Zhang, C. Stevenson, K. Ishara, R. Zhang, H. Zhu and J. Ma, *Adv. Funct. Mater.*, 2016, **26**, 7614–7625.
9 Z. Ma, Q. Huang, Q. Xu, Q. Zhuang, X. Zhao, Y. Yang, H. Qiu, Z. Yang, C. Wang, Y. Chai and Z. Zheng, *Nat. Mater.*, 2021, **20**, 859–868.
10 Y. Wang, W. Qin, X. Hu, Z. Liu, Z. Ren, H. Cao, B. An, X. Zhou, M. Shafiq, S. Yin and Z. Liu, *Sens. Actuators, B*, 2022, **368**, 132228.
11 A. Fakharuddin, H. Li, F. Di Giacomo, T. Zhang, N. Gasparini, A. Y. Elezzabi, A. Mohanty, A. Ramadoss, J. Ling, A. Soultati, M. Tountas, L. Schmidt-Mende, P. Argitis, R. Jose, M. K. Nazeeruddin, A. R. B. Mohd Yusoff and M. Vasilopoulou, *Adv. Energy Mater.*, 2021, **11**, 2101443.
12 L. Wang, X. Fu, J. He, X. Shi, T. Chen, P. Chen, B. Wang and H. Peng, *Adv. Mater.*, 2020, **32**, 1901971.
13 F. Mo, G. Liang, Z. Huang, H. Li, D. Wang and C. Zhi, *Adv. Mater.*, 2020, **32**, 1902151.
14 J. Xiong, J. Chen and P. S. Lee, *Adv. Mater.*, 2021, **33**, 2002640.

15 H. Peng, *Adv. Mater.*, 2020, **32**, e1904697.
16 X. Xu, S. Xie, Y. Zhang and H. Peng, *Angew. Chem., Int. Ed.*, 2019, **58**, 13643–13653.
17 H. Sun, Y. Zhang, J. Zhang, X. Sun and H. Peng, *Nat. Rev. Mater.*, 2017, **2**, 17023.
18 W. Song, Z. Bie, W. Yan, J. Zhu and W. Ma, *EcoMat*, 2022, **4**, e12177.
19 S. Xiang, N. Zhang and X. Fan, *Adv. Fiber Mater.*, 2021, **3**, 76–106.
20 H. Cheng, Q. Li, L. Zhu and S. Chen, *Small Methods*, 2021, **5**, 2100502.
21 N. Sheng, S. Chen, J. Yao, F. Guan, M. Zhang, B. Wang, Z. Wu, P. Ji and H. Wang, *Chem. Eng. J.*, 2019, **368**, 1022–1032.
22 T. Xiong, B. He, T. Zhou, Z. Wang, Z. Wang, J. Xin, H. Zhang, X. Zhou, Y. Liu and L. Wei, *EcoMat*, 2022, **4**, e12218.
23 L. Huang, S. Lin, Z. Xu, H. Zhou, J. Duan, B. Hu and J. Zhou, *Adv. Mater.*, 2020, **32**, 1902034.
24 K. Liu, Z. Chen, T. Lv, Y. Yao, N. Li, H. Li and T. Chen, *Nano-Micro Lett.*, 2020, **12**, 64.
25 T. Stockinger, D. Wirthl, G. Mao, M. Drack, R. Pruckner, S. Demchyshyn, M. Steiner, F. Egger, U. Müller, R. Schwödiauer, S. Bauer, N. Arnold and M. Kaltenbrunner, *Adv. Mater.*, 2021, **33**, 2170293.
26 M. M. Alam, S. Lee, M. Kim, K. S. Han, V. A. Cao and J. Nah, *Nano Energy*, 2020, **72**, 104672.
27 Y. Zhang, X. Li, J. Kim, Y. Tong, E. G. Thompson, S. Jiang, Z. Feng, L. Yu, J. Wang, D. S. Ha, H. Sontheimer, B. N. Johnson and X. Jia, *Adv. Opt. Mater.*, 2021, **9**, 2001815.
28 T. Jia, Y. Wang, Y. Dou, Y. Li, M. J. Andrade, R. Wang, S. Fang, J. Li, Z. Yu, R. Qiao, Z. Liu, Y. Cheng, Y. Su, M. Minary-Jolandan, R. H. Baughman, D. Qian and Z. Liu, *Adv. Funct. Mater.*, 2019, 1808241.
29 Y. Cheng, R. Wang, K. H. Chan, X. Lu, J. Sun and G. W. Ho, *ACS Nano*, 2018, **12**, 3898–3907.
30 X. Leng, X. Zhou, J. Liu, Y. Xiao, J. Sun, Y. Li and Z. Liu, *Mater. Horiz.*, 2021, **8**, 1538.
31 Z. Wang, J. Cheng, Q. Guan, H. Huang, Y. Li, J. Zhou, W. Ni, B. Wang, S. He and H. Peng, *Nano Energy*, 2018, **45**, 210–219.
32 J. Lee, S. J. Ihle, G. S. Pellegrino, H. Kim, J. Yea, C.-Y. Jeon, H.-C. Son, C. Jin, D. Eberli, F. Schmid, B. L. Zambrano, A. F. Renz, C. Forró, H. Choi, K.-I. Jang, R. Küng and J. Vörös, *Nat. Electron.*, 2021, **4**, 291–301.
33 Z. Liu, D. Qi, G. Hu, H. Wang, Y. Jiang, G. Chen, Y. Luo, X. J. Loh, B. Liedberg and X. Chen, *Adv. Mater.*, 2018, **30**, 1704229.
34 Z. Liu, T. Zhu, J. Wang, Z. Zheng, Y. Li, J. Li and Y. Lai, *Nano-Micro Lett.*, 2022, **14**, 61.
35 S. J. Kim, D. H. Shin, Y. S. Choi, H. Rho, M. Park, B. J. Moon, Y. Kim, S.-K. Lee, D. S. Lee, T.-W. Kim, S. H. Lee, K. S. Kim, B. H. Hong and S. Bae, *ACS Nano*, 2018, **12**, 2803–2808.
36 J. Lee, B. Llerena Zambrano, J. Woo, K. Yoon and T. Lee, *Adv. Mater.*, 2020, **32**, 1902532.
37 T. Agcayazi, K. Chatterjee, A. Bozkurt and T. K. Ghosh, *Adv. Mater. Technol.*, 2018, **3**, 1700277.
38 N. Zhou, B. Jiang, X. He, Y. Li, Z. Ma, H. Zhang and M. Zhang, *ACS Appl. Mater. Interfaces*, 2021, **13**, 19254–19262.
39 Y. Cheng, H. Zhang, R. Wang, X. Wang, H. Zhai, T. Wang, Q. Jin and J. Sun, *ACS Appl. Mater. Interfaces*, 2016, **8**, 32925–32933.
40 Z. Zhang, Z. Yang, J. Deng, Y. Zhang, G. Guan and H. Peng, *Small*, 2015, **11**, 675–680.
41 J. Yu, W. Lu, J. P. Smith, K. S. Booksh, L. Meng, Y. Huang, Q. Li, J.-H. Byun, Y. Oh, Y. Yan and T.-W. Chou, *Adv. Energy Mater.*, 2017, **7**, 1600976.
42 Y. Xu, Y. Zhao, J. Ren, Y. Zhang and H. Peng, *Angew. Chem., Int. Ed.*, 2016, **55**, 7979–7982.
43 Y. Cheng, X. Lu, K. H. Chan, R. Wang, Z. Cao, J. Sun and G. W. Ho, *Nano Energy*, 2017, **41**, 511–518.
44 F. Guan, Z. Han, M. Jin, Z. Wu, Y. Chen, S. Chen and H. Wang, *Adv. Fiber Mater.*, 2021, **3**, 128–137.
45 Z. F. Liu, S. Fang, F. A. Moura, J. N. Ding, N. Jiang, J. Di, M. Zhang, X. Lepró, D. S. Galvão, C. S. Haines, N. Y. Yuan, S. G. Yin, D. W. Lee, R. Wang, H. Y. Wang, W. Lv, C. Dong, R. C. Zhang, M. J. Chen, Q. Yin, Y. T. Chong, R. Zhang, X. Wang, M. D. Lima, R. Ovalle-Robles, D. Qian, H. Lu and R. H. Baughman, *Science*, 2015, **349**, 400–404.
46 F. Sun, M. Tian, X. Sun, T. Xu, X. Liu, S. Zhu, X. Zhang and L. Qu, *Nano Lett.*, 2019, **19**, 6592–6599.
47 L. Zheng, M. Zhu, B. Wu, Z. Li, S. Sun and P. Wu, *Sci. Adv.*, 2021, **7**, eabg4041.
48 Y. Sun, B. Gates, B. Mayers and Y. Xia, *Nano Lett.*, 2002, **2**, 165–168.
49 J. Jiu, K. Murai, D. Kim, K. Kim and K. Suganuma, *Mater. Chem. Phys.*, 2009, **114**, 333–338.
50 T. Araki, J. Jiu, M. Nogi, H. Koga, S. Nagao, T. Sugahara and K. Suganuma, *Nano Res.*, 2014, **7**, 236–245.
51 S. Lee, S. Shin, S. Lee, J. Seo, J. Lee, S. Son, H. J. Cho, H. Algadi, S. Al-Sayari, D. E. Kim and T. Lee, *Adv. Funct. Mater.*, 2015, **25**, 3114–3121.
52 S. Zhang, Z. He, G. Zhou, B.-M. Jung, T.-H. Kim, B.-J. Park, J.-H. Byun and T.-W. Chou, *Compos. Sci. Technol.*, 2020, **189**, 108011.
53 Y. Lu, J. Jiang, S. Yoon, K.-S. Kim, J.-H. Kim, S. Park, S.-H. Kim and L. Piao, *ACS Appl. Mater. Interfaces*, 2018, **10**, 2093–2104.
54 C. Lu, S. Park, T. J. Richner, A. Derry, I. Brown, C. Hou, S. Rao, J. Kang, C. T. Moritz, Y. Fink and P. Anikeeva, *Sci. Adv.*, 2017, **3**, e1600955.
55 A. Kim, J. Ahn, H. Hwang, E. Lee and J. Moon, *Nanoscale*, 2017, **9**, 5773–5778.
56 Z. Cao, R. Wang, T. He, F. Xu and J. Sun, *ACS Appl. Mater. Interfaces*, 2018, **10**, 14087–14096.
57 Y. Qu, T. Nguyen-Dang, A. G. Page, W. Yan, T. Das Gupta, G. M. Rotaru, R. M. Rossi, V. D. Favrod, N. Bartolomei and F. Sorin, *Adv. Mater.*, 2018, **30**, 1707251.
58 K. Yadav, S. Jha, M. Jassal and A. K. Agrawal, *Polymer*, 2019, **169**, 46–51.
59 H.-Y. Liu, H.-C. Hsieh, J.-Y. Chen, C.-C. Shih, W.-Y. Lee, Y.-C. Chiang and W.-C. Chen, *Macromol. Chem. Phys.*, 2019, **220**, 1800387.
60 Y. Cheng, R. Wang, H. Zhai and J. Sun, *Nanoscale*, 2017, **9**, 3834–3842.
61 Y. Zhao, D. Dong, S. Gong, L. Brassart, Y. Wang, T. An and W. Cheng, *Adv. Electron. Mater.*, 2019, **5**, 1800462.